Variability and trends in sea ice extent and ice production in the Ross Sea

Josefino C. Comiso,[1] Ronald Kwok,[2] Seelye Martin,[3] and Arnold L. Gordon[4]

Received 7 May 2010; revised 6 December 2010; accepted 24 January 2011; published 21 April 2011.

[1] Salt release during sea ice formation in the Ross Sea coastal regions is regarded as a primary forcing for the regional generation of Antarctic Bottom Water. Passive microwave data from November 1978 through 2008 are used to examine the detailed seasonal and interannual characteristics of the sea ice cover of the Ross Sea and the adjacent Bellingshausen and Amundsen seas. For this period the sea ice extent in the Ross Sea shows the greatest increase of all the Antarctic seas. Variability in the ice cover in these regions is linked to changes in the Southern Annular Mode and secondarily to the Antarctic Circumpolar Wave. Over the Ross Sea shelf, analysis of sea ice drift data from 1992 to 2008 yields a positive rate of increase in the net ice export of about 30,000 km^2 yr^{-1}. For a characteristic ice thickness of 0.6 m, this yields a volume transport of about 20 km^3 yr^{-1}, which is almost identical, within error bars, to our estimate of the trend in ice production. The increase in brine rejection in the Ross Shelf Polynya associated with the estimated increase with the ice production, however, is not consistent with the reported Ross Sea salinity decrease. The locally generated sea ice enhancement of Ross Sea salinity may be offset by an increase of relatively low salinity of the water advected into the region from the Amundsen Sea, a consequence of increased precipitation and regional glacial ice melt.

Citation: Comiso, J. C., R. Kwok, S. Martin, and A. L. Gordon (2011), Variability and trends in sea ice extent and ice production in the Ross Sea, *J. Geophys. Res.*, *116*, C04021, doi:10.1029/2010JC006391.

1. Introduction

[2] The Ross Sea is of considerable interest because as described herein, it is one of the few regions in the Southern Ocean identified by satellite data as experiencing a significant positive trend in sea ice extent and a negative trend in sea surface temperature [*Comiso*, 2010, Figures 10.7d and 10.8d]. Some studies associate this phenomenon with the El Niño–Southern Oscillation (ENSO), and the Southern Annular Mode (SAM) either independently or in combination [*Kwok and Comiso*, 2002; *Ledley and Huang*, 1997; *Stammerjohn et al.*, 2008]. *Turner et al.* [2009] reported in a modeling study that the ozone hole causes amplification of the polar lows, especially in autumn in the Western Antarctic, which in turn causes strong winds to form in the vicinity of the Ross Ice Shelf. Also, *Gille* [2002] observed a warming of the intermediate water in the Southern Ocean that she attributes in part to the changing phase of SAM. Other phenomenological studies show significant warming trends over the West Antarctic ice sheet suggesting overall influences of the increasing atmospheric greenhouse gases on a long-term basis [*Steig et al.*, 2009].

[3] In the Ross Sea, there are three persistent polynyas: the Ross Shelf Polynya (RSP) that forms along the Ross Ice Shelf to the east of Ross Island and two relatively minor polynyas that form in Terra Nova Bay to the north of the Drygalski Ice Tongue and McMurdo Sound [*Bromwich and Kurtz*, 1982, 1984; *Martin et al.*, 2007; *Fusco et al.*, 2009]. The RSP is the largest Antarctic coastal polynya, where *Martin et al.* [2007] estimate its mean winter area to be ~25,000 km^2, while the smaller Terra Nova Bay polynya has a mean area of ~3000 km^2. The RSP in particular is associated with the formation of high-salinity shelf water (HSSW) [*Zwally et al.*, 1985; *Jacobs and Comiso*, 1989; *Martin et al.*, 2007]. The reason that this polynya is a prime source of HSSW, a major ingredient of Antarctic Bottom Water (ABW), is the presence of an extensive ocean shelf region adjacent to the ice shelf that allows for the HSSW buildup. Through almost continuous formation and export of sea ice at the shelf during autumn and winter, the shelf water salinity is enhanced until it attains densities that contribute to the ABW. The mechanisms for the production and export to the deep ocean of ABW from the Ross Sea and interannual changes in the export rate have been studied as part of the Antarctic Slope (AnSlope) project [*Gordon*

[1]Cryospheric Sciences Branch, NASA Goddard Space Flight Center, Greenbelt, Maryland, USA.
[2]Jet Propulsion Laboratory, California Institute of Technology, Pasadena, California, USA.
[3]School of Oceanography, University of Washington, Seattle, Washington, USA.
[4]Lamont-Doherty Earth Observatory, Columbia University, Palisades, New York, USA.

0148-0227/11/2010JC006391

et al., 2009]. For the years 1992–2002, *Martin et al.* [2007] calculate the ice production in the Ross Sea polynyas and show that for the giant Ross Shelf Polynya (RSP), some of the changes in ice production are associated with the iceberg calving events. This paper used the ECMWF (European Center for Medium-Range Weather Forecasts) 40 year reanalysis (ERA-40) data set, which covers the period 1957–2002. In the present paper, to extend the time series to 2008, we use the ECMWF daily operational analysis to recalculate the heat fluxes and winds for the entire period, while using for 1992–2002, the same polynya areas derived by *Martin et al.* [2007]. This change in the meteorological data set creates some differences in the annual ice production between the two papers. *Tamura et al.* [2008] and *Kern* [2009] also study the RSP; these papers obtain different results. Section 4 below discusses in detail the reasons for these differences.

[4] The much smaller Terra Nova Bay polynya is also considered a producer of HSSW because of intense air–sea ice interactions in the region. Hydrographic studies [e.g., *Budillon et al.*, 2003; *Gordon et al.*, 2009; *Orsi and Wiederwohl*, 2009] that analyzed the physical properties of the bottom layers showed a clear salinity gradient extending from the TNB polynya that confirmed its role in HSSW production.

[5] It is intriguing that while the ice cover in the Bellingshausen/Amundsen seas is declining, the ice cover in primarily the western Ross Sea is increasing [*Zwally et al.*, 2002; *Comiso and Nishio*, 2008; *Comiso*, 2010]. As *Comiso* [2010] shows, this areal increase is consistent with the decrease in surface temperature that occurs in the western Ross Sea. Meanwhile, the rest of the ice cover around Antarctica has been increasing but at a more modest rate. The net increase in the Antarctic ice cover as inferred from satellite data is thus mainly due to the ice cover increase in the Ross Sea. A question of interest is whether this phenomenon is associated with an overall increase in ice production in the Ross Sea region. A related question is whether the rate of bottom water formation in the Ross Sea is changing as well. In this study, we make use of about 30 years of satellite passive microwave data to quantify recent changes and trends in the ice cover of the Ross Sea and adjacent areas. Temporal changes in the ice production of the Ross Sea coastal polynya are quantified and used to estimate yearly ice production and salinization. Because the Ross Sea lacks natural seaward boundaries, its ice cover is studied in conjunction with changes in adjacent regions as well as for the entire Antarctic region. The general characteristics and interannual changes in the regional ice drift as observed by satellite are also presented with a view of assessing ice production independently and determining how dynamics affects the distribution and interannual changes in the ice cover.

2. Environmental Setting and Satellite Observations

[6] Figure 1a shows the ice cover during minimum (dark gray) and maximum (light gray) extents. The location of the longitudinal boundaries of the sea ice sectors around Antarctica as defined previously by *Zwally et al.* [1983] are indicated by the solid lines (numbered 1 to 5) in Figure 1a and will be adopted in this study. For Antarctica, the Weddell Sea has the most extensive winter ice cover, with the Ross Sea second in extent.

[7] Figure 1b, the bathymetry of the Southern Ocean, shows that relatively shallow shelf regions surround Antarctica, with the largest shelf areas occurring in the Western Weddell and the Ross seas. During summer, the sea ice cover is generally located over these shallow shelf regions. The only exception to this occurs in the Ross Sea where during spring, a coastal polynya usually forms adjacent to the ice shelf, then during summer, expands north toward the ice edge. In all regions during winter, the ice cover advances to the north; for the Ross Sea, the ice edge usually does not go beyond the Pacific Antarctic ridge crest (around 60°S). It is likely that during winter, the steering of the ocean circulation by the seafloor bathymetry [*Gordon et al.*, 1978] is in part responsible for the occurrence of a sharp rectangular corner in the ice cover at about 145°W and 60°S shown in Figure 1a.

[8] Atmospheric and oceanographic conditions are the primary factors influencing the growth and decay of sea ice. In autumn, the rapid decline in surface air temperature cools the open ocean leading to frazil ice formation. As long as the surface temperature remains at the freezing point, sea ice forms and advances northward. When this condition is no longer satisfied, the ice retreats to the south owing to warmer air or to lateral and vertical ocean heat flux.

[9] The location of the surface temperature isotherms are influenced by the atmospheric circulation that is primarily associated with changes of the Southern Annular Mode (SAM) [*Thompson and Solomon*, 2002; *Hall and Visbeck*, 2002]. Figures 1c and 1d show multiyear averages of the distribution of sea surface temperature (SST) as derived from AVHRR data for 1979 to 2008 and for February and September, respectively. It is apparent that the shape of the near-freezing temperature isotherms are similar to those of the sea ice edge. For the same months, average wind vectors, derived from the National Centers for Environmental Prediction- National Center for Atmospheric Research (NCEP-NCAR) reanalysis data [*Kalnay et al.*, 1996], are overlain on Figures 1c and 1d. Winds not only influence the surface temperature but also drive the Antarctic circumpolar current and the distribution of the ice cover. The strong southerly winds off the Ross Ice Shelf that occur in spring and summer generate the spring coastal polynya and during most summers cause the Ross Sea to have little or no ice cover.

[10] The primary tool for large-scale variability studies of the ice cover is the passive microwave data set that has provided continuous data since November 1978. These data provide day/night observation of the entire sea ice cover at a relatively good temporal resolution. The basic data are daily averages gridded in a polar stereographic format. The source of this data is the Nimbus-7 Scanning Multichannel Microwave Radiometer (SMMR) and the DMSP/Special Scanning Microwave Imager (SSM/I), both with a 25 km resolution, and the AQUA/Advanced Multichannel Scanning Radiometer-EOS (AMSR-E), with a 12.5 km resolution. For consistency, we use the continuous multichannel data from SMMR (November 1978 to July 1987) and SSM/I (July 1987 to the present) for interannual and trend analysis. Although AMSR-E provides better resolution and more

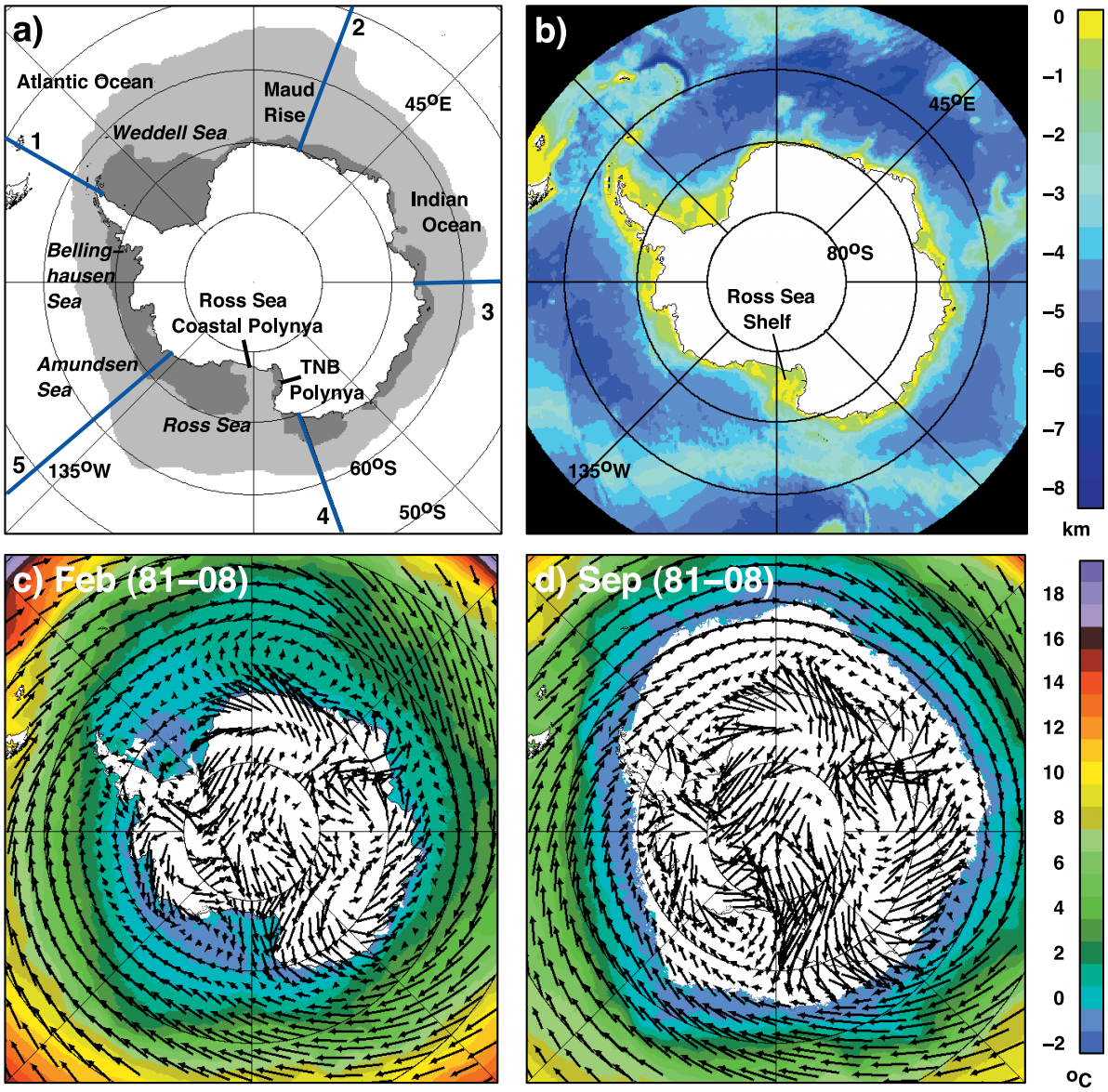

Figure 1. (a) Location map of the Southern Ocean, longitudinal boundaries of the sectors (numbered blue lines), and the climatological monthly averages of the Antarctic Sea ice cover in February (dark gray) and September (light gray). (b) Color-coded bathymetry of the Southern Ocean (from the General Bathymetric Chart of the Oceans (GEBCO) 1 min grid, version 2.0; see http://www.gebco.net). (c) Color-coded sea surface temperature average in February (1979–2008) with average wind vectors from NCEP overlain. (d) Color-coded sea surface temperature in September (1979–2008) with average wind vectors overlain.

accurate data, *Comiso and Nishio* [2008] show that SMMR and SSM/I data provide similar ice concentrations and long-term and consistent representation of the ice cover.

[11] During the overlap period of SSM/I and AMSR-E from June 2002 to the present, although analysis of the two data sets yielded similar results, there are subtle differences associated with resolution such as the location of the ice edges including those of polynyas (by a few km). We took advantage of the higher-resolution AMSR-E data to test the effect of resolution and to ensure that the overall results are not resolution-dependent.

[12] The main parameter derived from passive microwave data is sea ice concentration, which is generated using an algorithm that takes advantage of the contrast in the emissivity of sea ice and open water at different frequencies. The two algorithms used most frequently are the Bootstrap Algorithm discussed by *Comiso* [2009] and the NT2 Algorithm discussed by *Markus and Cavalieri* [2009]. *Parkinson and Comiso* [2008] compare the concentration data from the two algorithms and show that they yield similar results. These algorithms have also been validated against field and high-resolution satellite data and the results show accuracies

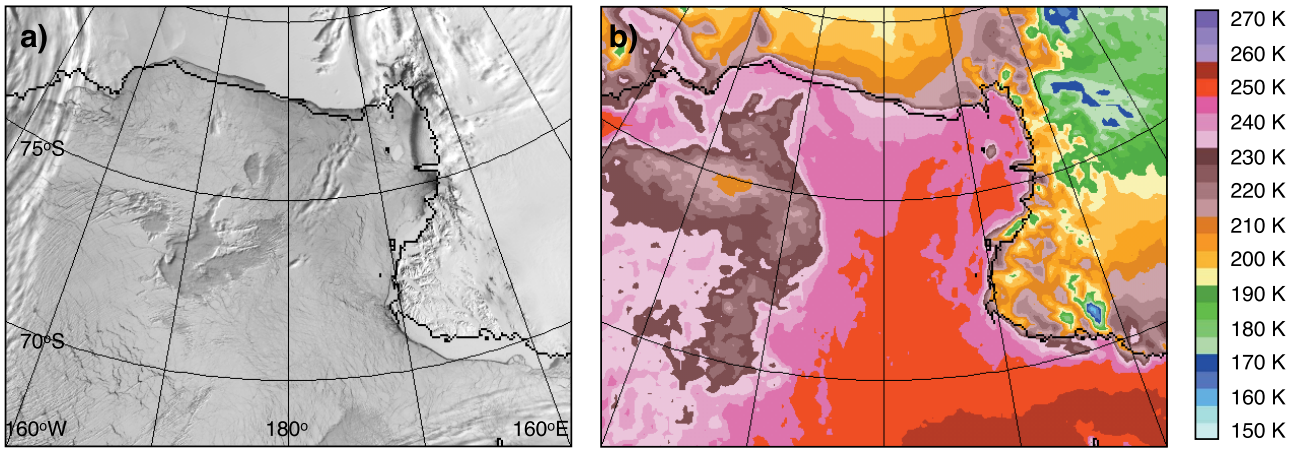

Figure 2. Coincident images of the Ross Sea region from (a) Aqua/MODIS (0.65 μm channel) and (b) Aqua/AMSR-E (37 GHz brightness temperature at vertical polarization) on 12 October 2007. The black line shows the published shelf/ocean boundary [*Defense Mapping Agency*, 1992].

ranging generally from 5% to 15% depending on location and season. The errors are larger near the ice edge and in coastal areas because of large variability of the emissivity of sea ice in these regions. For improved interpretation, we supplement the passive microwave data with other satellite data sets including high-resolution visible, infrared and synthetic aperture radar (SAR) data. In this study, we derive the ice concentration data from November 1978 to December 2009 using the Bootstrap Algorithm. Unfortunately, the NT2 algorithm requires the 85 GHz data that are not available with SMMR (November 1978 to August 1987) and parts of the SSM/I data set (February 1989 to December 1991). This ice concentration data is used to estimate the fraction of open water within the ice pack and to estimate the ice extent, which is the integrated sum of the area of all grid cells containing at least 15% ice. It is also used to estimate the ice area, which represents the total area actually covered by ice and is the integral sum of the products of the area of each grid cell with the corresponding ice concentration. The ice extent and ice area are generally used to quantify the variability and long-term trends of the ice cover.

[13] Because the signatures of sea ice and glacial ice are generally similar, it is difficult to develop an algorithm that discriminates one from the other. As a result, we normally used a land ice mask as described by *Comiso* [2009]. The use of a land ice mask however, is problematic especially in ice shelf and glacier regions where iceberg calving and ice surges are unpredictable. To illustrate this, concurrent high-resolution visible (250 m) images from Aqua/MODIS and microwave brightness temperature data at 37 GHz (vertical polarization) from Aqua/AMSR-E are presented in Figure 2a and 2b, respectively. These images were acquired over the Ross Sea region on 12 October 2007 after the calving of large icebergs in 2000 and 2002 [*Martin et al.*, 2007]. In both images, the solid black line shows the shelf/ocean boundary as published previously [*Defense Mapping Agency*, 1992]; it is apparent that because of the loss of shelf ice, the actual ice boundary at this time is south of the published boundary. Because of the importance of the shelf position, we used a mix of SAR and visible imagery to determine the location of the ice shelf front.

3. Ross Sea Ice Cover: Spatial Variability and Dynamics

[14] The focus of this study is the spatial distribution and general characteristics of the ice cover in the Ross Sea. However, since there is no obvious northern boundary to the Ross Sea and because the Ross sea ice is advected by winds and currents, our study is not complete without also studying the ice conditions in and the exchange of ice with the adjacent Amundsen/Bellingshausen seas.

3.1. Variability in Ice Extents and Ice Area in the Ross Sea and Adjacent Regions

[15] The Antarctic sea ice cover extent varies from a minimum of about 3×10^6 km^2 in summer to a maximum of about 18×10^6 km^2 in winter [*Zwally et al.*, 2002; *Comiso*, 2010]. At the end of summer, the ice that survives is referred to as perennial ice. Since the perennial ice is the mainstay of the ice cover, it is of interest to know how its location and extent changes with time. For 1979–2008, Figure 3 shows the minimum in the daily sea ice extent, where this minimum corresponds to the perennial ice.

[16] It is apparent that from 1979 through 1987, much of the coastal area on the western side of the Antarctic Peninsula was covered by an almost contiguous perennial ice cover. During the same period, the region north of the Ross Ice Shelf was basically ice-free. In 1988, the ice cover remained primarily in the same general region west of the Antarctic Peninsula but was broken into segments with a segment located in the Ross Sea, or further to the west than previously observed. In contrast, from 1989 to 1992, the west side of the Antarctic Peninsula was mainly ice-free and the perennial ice cover in the region was anomalously low. Such low ice cover continued through 1997, followed by a slight recovery in 1998, 1999 and 2000, a record high ice cover in 2001, then back to low values in 2002, 2003, 2004, 2007, and 2008.

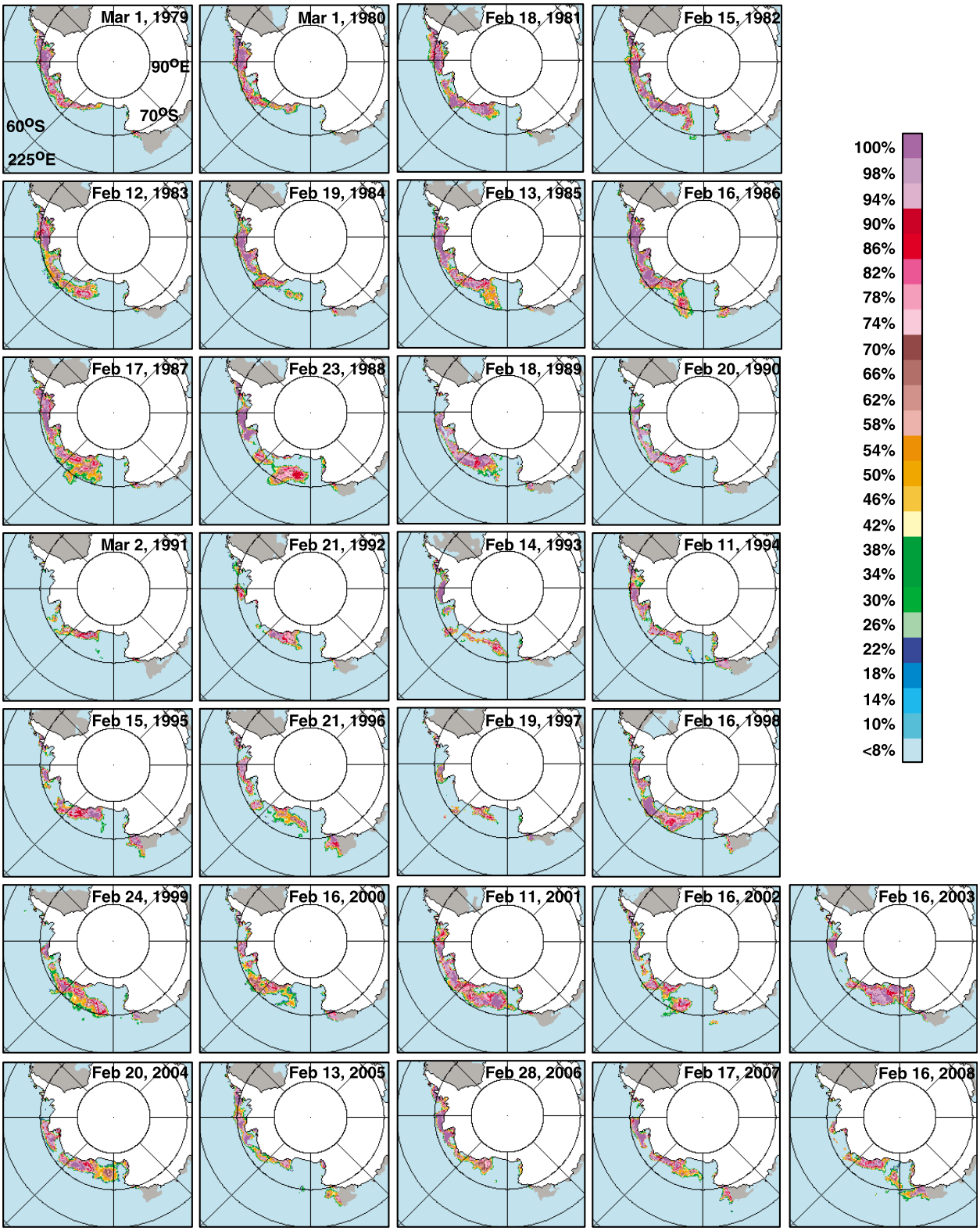

Figure 3. Color-coded sea ice concentration daily maps in the Ross Sea and Bellingshausen/Amundsen seas sector during summer minimum extents from 1979 to 2008. Gray shaded areas are parts of other Antarctic sectors.

[17] In 2001, 2003, and 2004, the perennial ice cover retreated to the west, covering much of the Ross Sea in front of the Ross Sea Ice Shelf. This was in part an effect of the large icebergs calving in 2000 and again in 2002. In 2005 and 2006, the ice cover shifted to the east while in 2008, there was practically no perennial ice cover in the Bellingshausen/Amundsen seas. Overall, the images show that the location of the perennial ice in the region was relatively predictable during the first decade of satellite data but after that, the distribution of perennial ice in the area became more random, and sometimes moved west into the Ross Sea.

[18] For comparison, Figure 4 shows the maximum in the daily sea ice extent. Figure 4 shows large variation with longitude of the northern ice edge position. It also shows that at each longitude, the edge location has a significant interannual variability. As indicated earlier, the regional ice cover has a strong tendency to form a rectangular corner at about 145°W. This rectangular feature is most apparent in 1983, 1985, 1991, 1992, 1996, 1998, 2000, 2002, 2003, and 2007. Its recurrence and persistence suggests that its unusual shape is associated with an oceanographic circulation feature coupled to the regional bathymetry [*Gordon et al.*, 1978]. Also, in the Ross Sea, the northern edge of the ice is almost linear and colocated with a bathymetric rise at the Pacific-Antarctic ridge that confines the ocean current mainly to a flow parallel to the ridge crest and thus restricts the advection of sea ice across the ridge. In addition, the ocean circulation would allow the warmer deep water to flow over the northern flank of the ridge, which may increase the deep-to-surface heat flux in that region, limiting the sea ice cover from advancing further. This would induce the sharp linear form of the ice edge from 145°W to 165°W that occurs in most years.

[19] The near linear ice edge that occurs in some years from 145°W to the tip of the Antarctic Peninsula lies primarily over the deep ocean, and may be a downstream advective projection of the ice pattern initiated over the Pacific-Antarctic ridge. Large departures from the rectangular corner shape occurred in 2004 when the circumpolar ice cover was almost circular, and in 2005 when the ice edge in the Amundsen Sea advanced only slightly in winter. There are years when the ice cover edge in the Bellingshausen Sea is closer to the peninsula than other years as is the case in 1983, 1988, 1989 and 1992. The poor correlation of the locations and extents of the winter ice cover to the previous summer ice cover suggests that the summer ice has little influence on the extent of the subsequent winter ice cover. Conditioning of the mixed layer of the ocean is therefore not a big factor and the interannual variability is likely driven primarily by ocean and atmosphere dynamics.

[20] To assess the yearly changes more quantitatively, Figure 5 presents hemispheric monthly sea ice anomaly maps for September of each year. Because of the circumpolar nature of the changes and the associated dynamics, interpretation of the anomaly maps is facilitated by examination of the entire Antarctic region. The set of maps shows patterns of alternating anomalies corresponding to the advance (greens and blues) and retreat (purples and reds) of sea ice along the ice edge. Such anomalies have been associated with the Antarctic Circumpolar Wave (ACW; see *White and Peterson* [1996]), which they describe as a mode 2 system propagating around the Antarctic every 8 years. This phenomenon was also observed to occur in the sea level pressure and surface temperature fields. The anomaly maps indicate that the mode 2 system occurred during 1982, 1985, 1987, 1989, 2005, and 2007. It is obvious however, from inspection of the winter sea ice edge during 1979, 1984, 2003, 2006, and 2008 (Figure 5), that the system can be mode 3. The aforementioned event of abnormal ice in 2005 (Figure 4) in the Amundsen Sea also appears as a negative anomaly in Figure 5 and is likely related to the ACW. It is interesting that during the 2005–2007 period, the negative anomaly persisted in the same area suggesting the occurrence of a stationary wave (instead of a propagating wave) during this period. For the same period, the anomalies in the Ross Sea region were consistently positive, moving only slightly to the east.

[21] To gain insight into the ACW phenomenon, for each month from November 1978 through December 2009, Figure 6 shows the location of the Antarctic ice edge with respect to a climatological latitudinal mean ice edge, and that is plotted at longitudinal intervals of one degree. The image is a typical Hovmöeller diagram and is color-coded such that greens and blues represent locations that are north of the mean, while those in oranges and reds represent locations south of the mean. The diagonal black line on Figure 6, labeled A and starting at about 1980 and ending about 1988, lies over green values. The line shows the propagation of the wave as it completely circumnavigates the Antarctic over an 8 year period. This is about the period inferred by *White and Peterson* [1996]. About 4 years later (at around 1984), a similar pattern indicated by line B appears as predicted but continuous propagation of the wave is not as apparent, especially at around 150°E.

[22] The situation becomes even more inconsistent for the succeeding periods as indicated by lines C, D, E and F. As indicated earlier, the shifts from mode 2 to mode 3 such as those in 1984 and 1990 (see Figure 5) make it difficult to maintain the pattern. For the period 1992 to 1999, some suggestions of a propagating wave (line D) are apparent but none similar to the 1980 to 1988 period. While Figure 5 suggests an interesting pattern of alternating interval of advancing and retreating ice edges around the circumpolar region, changes in the system mode make the propagation unpredictable. Some of the inconsistencies in the Hovmöeller diagram may be attributed to use of a 30 year mean to estimate the anomalies and the possibility that the time series may not be long enough to represent a stable value for the mean. Alternative concepts, including the existence of an Antarctic Dipole (ADP) associated with the Pacific South American pattern (PSA) have been postulated [*Yuan and Li*, 2008]. Impacts of ENSO and the ozone hole also affect the atmospheric circulation [e.g., *Turner et al.*, 2009] and may in part cause the climate mode to be less predictable. The dominant effect of the Southern Annular Mode (SAM) however, has to be considered in any Antarctic sea ice circulation studies [*Hall and Visbeck*, 2002].

[23] To assess the interannual variability of the ice extent, Figure 7 shows the plots of the monthly ice extent anomalies for the entire Antarctic region and for the different sectors in Figure 1a. These plots are updates to those presented in the work of *Comiso and Nishio* [2008] and extend through

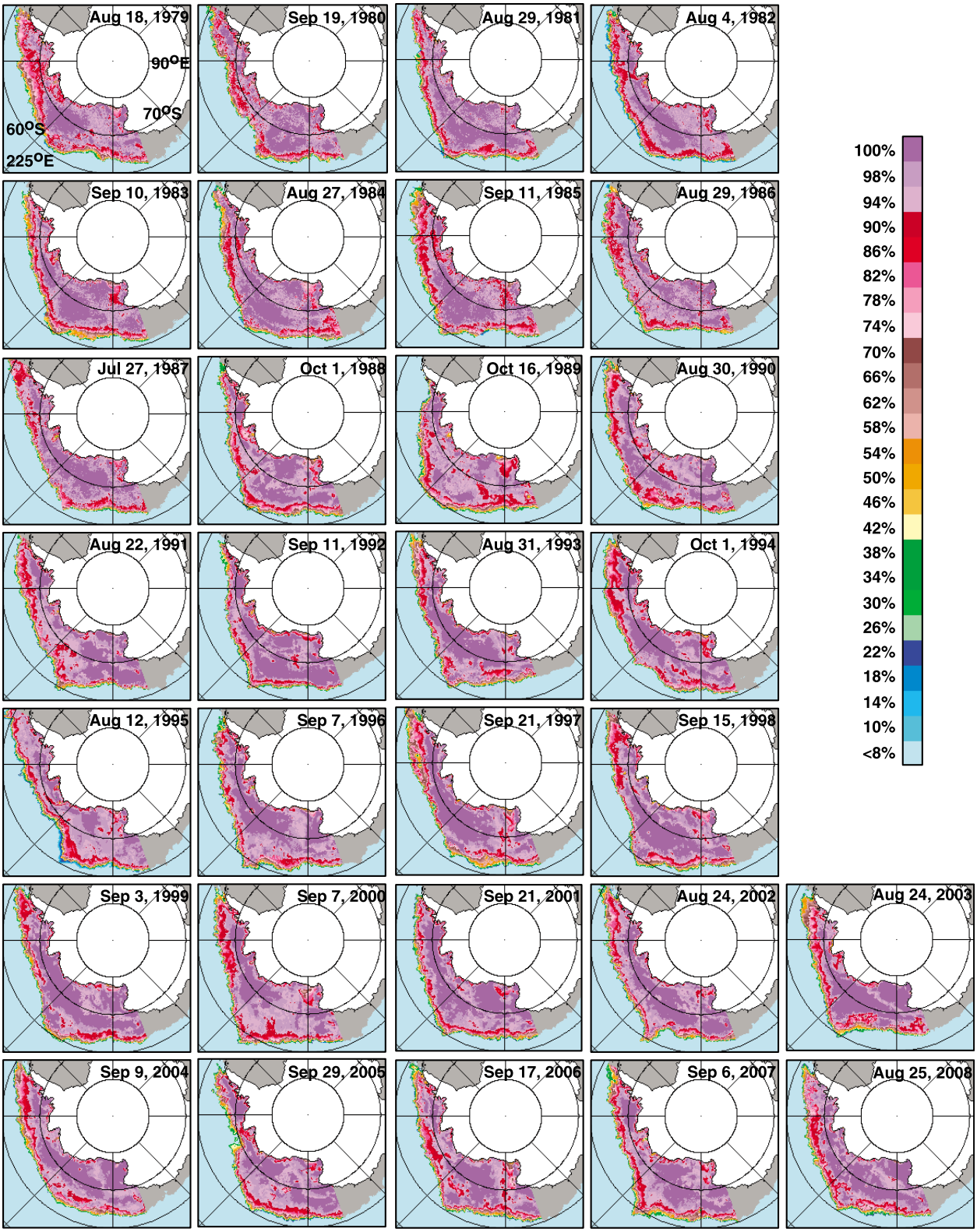

Figure 4. Color-coded sea ice concentration daily maps in the Ross Sea and Bellingshausen/Amundsen seas sectors during winter maximum extents from 1979 to 2008. Gray shaded areas are covered by sea ice but are parts of other Antarctic sectors.

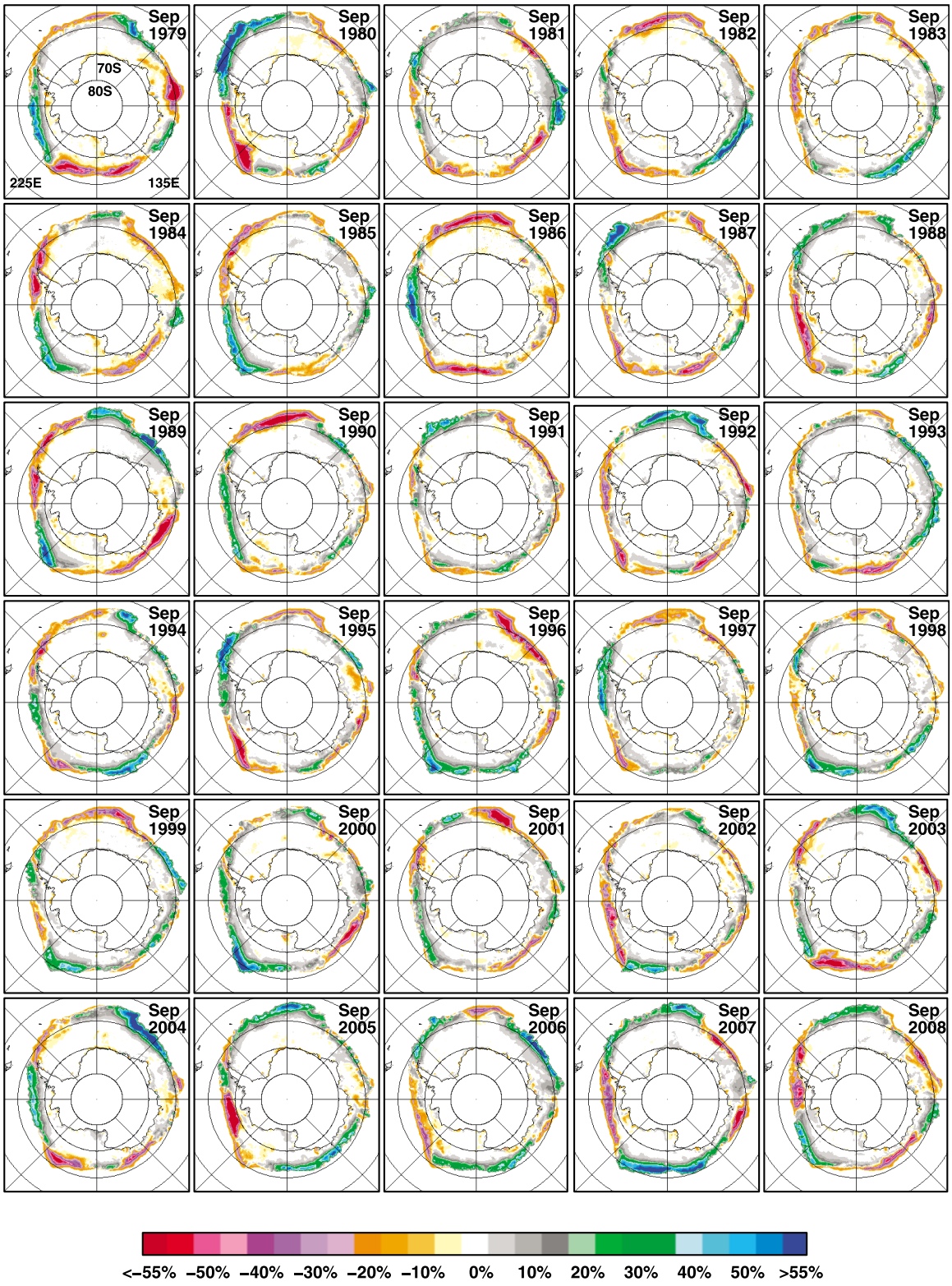

Figure 5. Color-coded sea ice concentration monthly anomaly maps for the entire Antarctic region during winter (i.e., September) from 1979 to 2008.

2008. For the entire Southern Ocean, the monthly anomaly plot in Figure 7a shows significant fluctuations as high as 1×10^6 km^2 and a linear regression of the data points yields a trend of 1.2 ± 0.2%/decade. The Weddell Sea and the West Pacific Ocean sectors show similar trends of 1.3 ± 0.5 and 0.9 ± 0.7%/decade, respectively, while the Indian Ocean sector shows a higher trend of 2.1 ± 0.6%/decade. In contrast to these relatively small and similar trends, the trend in

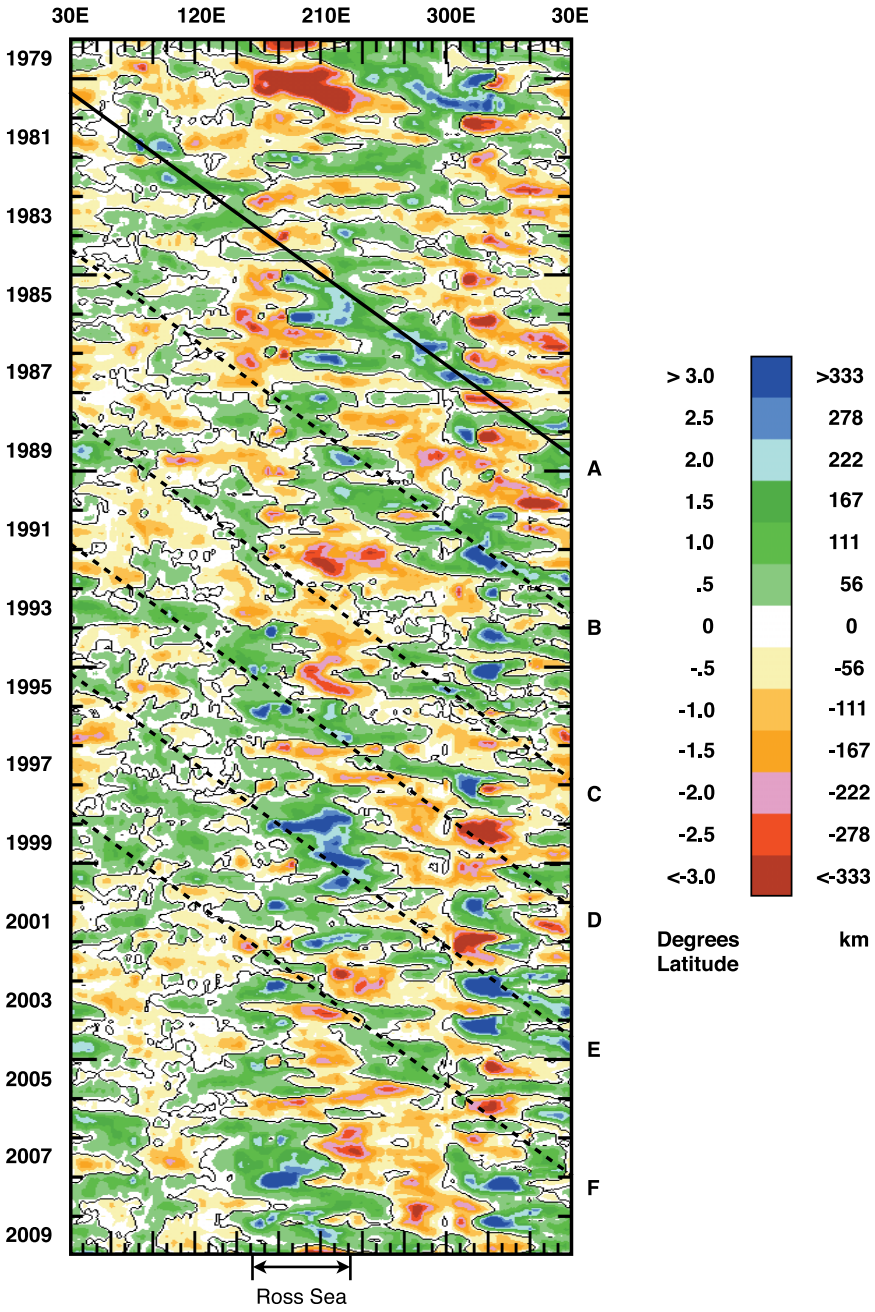

Figure 6. Antarctic circumpolar ice edge variability along 1° longitudes starting at 30°E for every month from 1979 to 2009. The greens and blues correspond to ice edges north of climatological ice edges, while the oranges and reds are those to south of the climatology. See text for definition of lines A–F.

the Ross Sea is about 5.0 ± 0.6%/decade while that of the Bellingshausen/Amundsen seas is about −7.1% ± 0.9%/decade. The Bellingshausen/Amundsen seas sector is adjacent to the Antarctic Peninsula that has been referred to as a climatologically anomalous region [*Jacobs and Comiso*, 1997; *King and Harangozo*, 1998]. The record ice cover retreat in the region in 1989 and 2005 illustrated in Figure 5 was also identified by *Jacobs and Comiso* [1989] and *Massom et al.* [2008]. *Massom et al.* [2008] show that the retreat in 2005 coincided with a strong and persistent northerly airflow that led to an extreme regional ice compaction. As Figure 3 shows, such compaction may have led to the recovery of the perennial ice in the Bellingshausen/Amundsen seas region in the subsequent summer (i.e., February 2006).

[24] The asymmetry in the trends of the ice cover extent in the Bellingshausen/Amundsen seas and Ross Sea is especially intriguing since the two sectors are adjacent. To gain insight into this phenomenon, Figure 8 shows plots of monthly ice extent, ice area and ice concentration of the combined Ross and Bellingshausen/Amundsen seas sector updated to 2010 (Figures 8a–8c). As expected, the

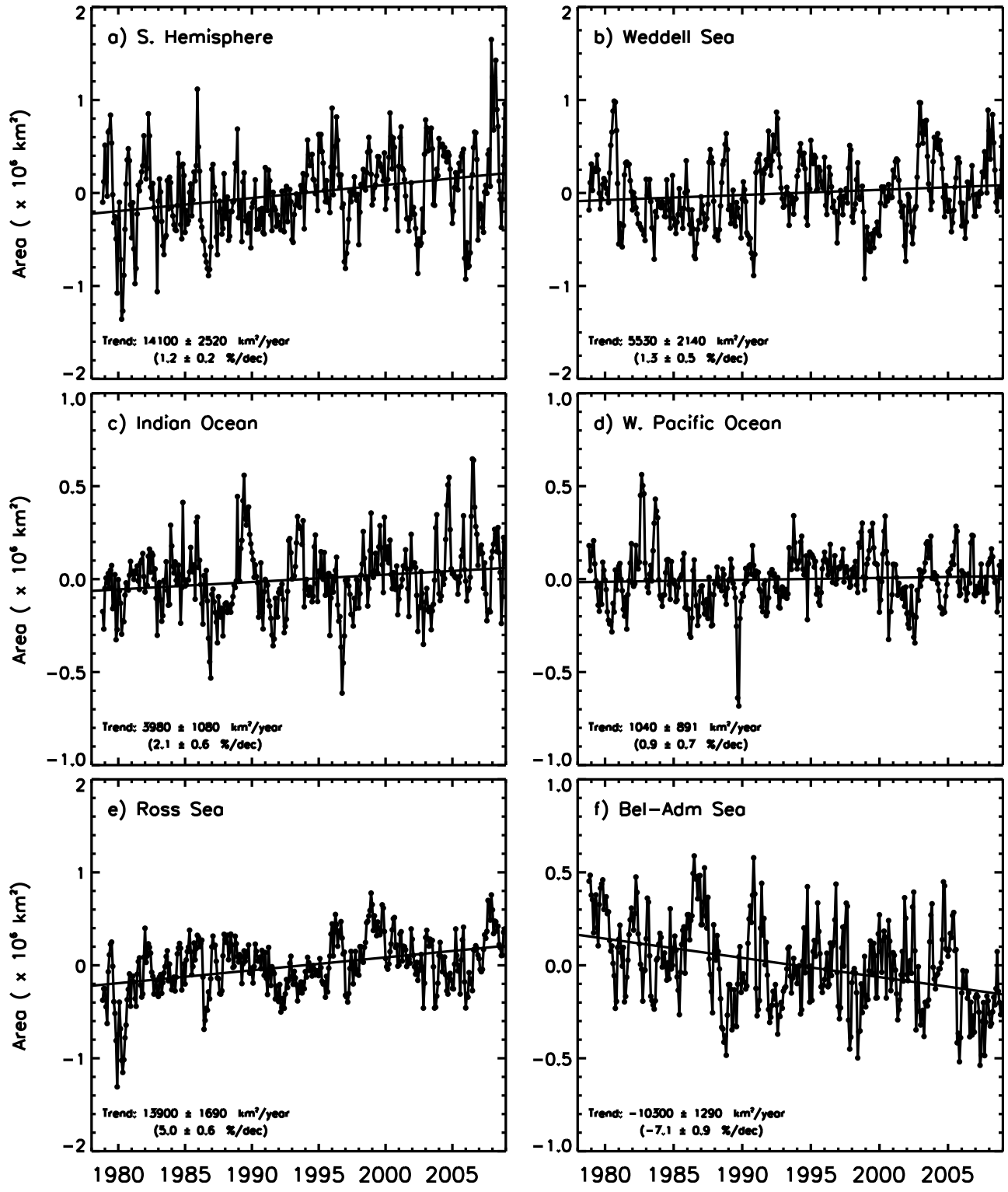

Figure 7. Plots of monthly ice extent anomalies in the (a) entire Southern Ocean, (b) Weddell Sea, (c) Indian Ocean, (d) West Pacific Ocean, (e) Ross Sea, and (f) Bellingshausen/Amundsen seas.

seasonal fluctuation is large, with the minimum and maximum averages in ice extent and area ranging from about 1.5 to 6 × 10^6 km^2 in ice extent and from 1 to 5.5 × 10^6 km^2 in ice area. It is also apparent that the interannual fluctuations of the peaks and valleys in extent and area are large, at ~1 × 10^6 km^2. Such large fluctuations are likely a response to interannual changes in atmospheric circulation. During the summer minimum period, this is also manifested in the ice-

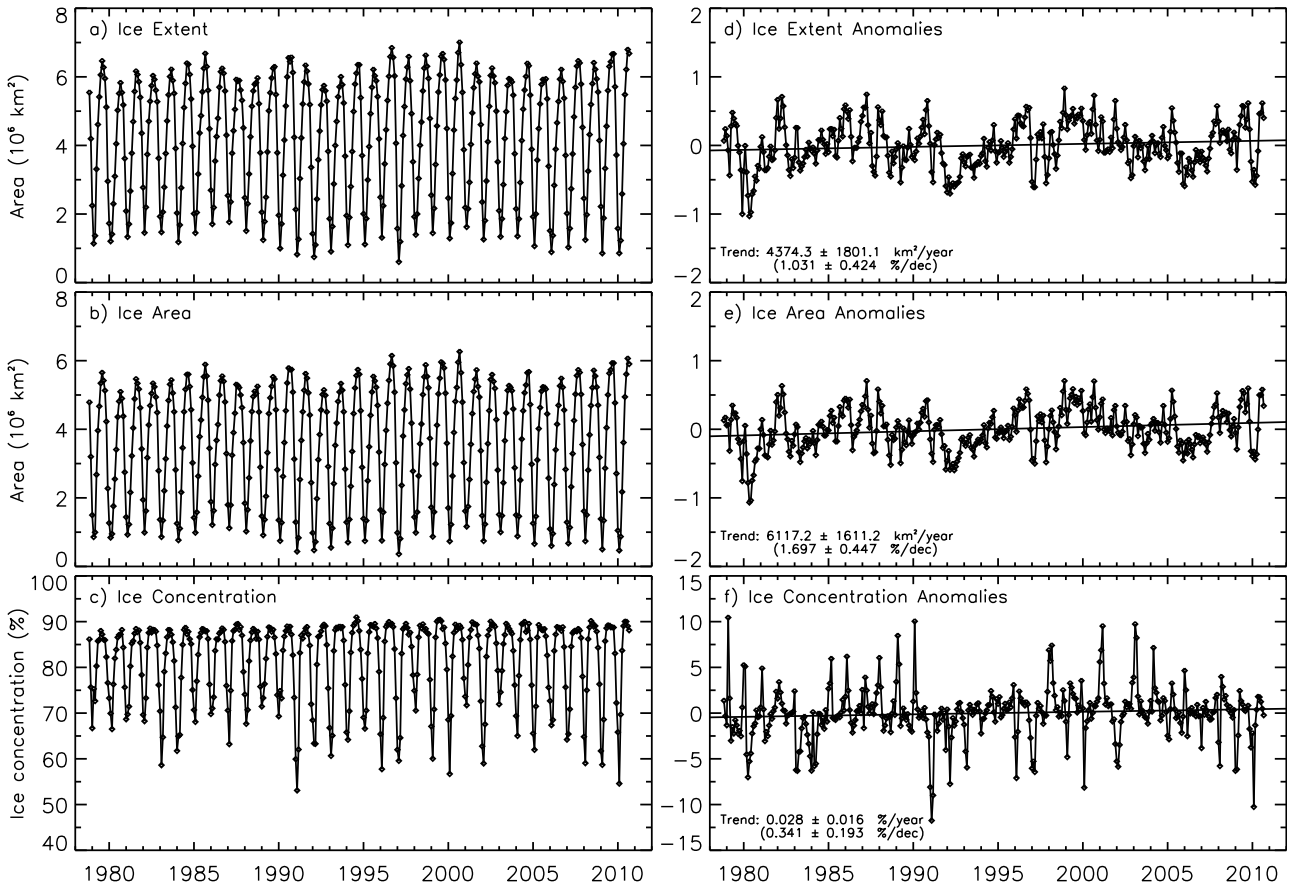

Figure 8. Plots of averages of monthly (a) ice extent, (b) ice area, and (c) ice concentration and monthly anomalies of (d) ice extent, (e) ice area, and (f) ice concentration of combined Ross Sea and Bellingshausen/Amundsen seas sectors. Thin solid lines represent linear regression fits to the data points in the anomaly plots and are used to estimate the trends in ice extents.

covered regions by the large variability of ice concentrations. This variability suggests that the processes associated with the asymmetry of the ice cover in the Ross and the Bellingshausen/Amundsen seas are not simply caused by ice advection from east to west or vice versa. The influence of the Antarctic perennial ice cover is also unlikely to be a big factor because during autumn and winter, the perennial ice is usually advected north to warmer waters where it melts.

[25] Figures 8d–8f present plots of the anomalies in ice extent, ice area and ice concentration; it is apparent that the interannual changes go through different phases of positive and negative anomalies but not in a periodic manner. The trend in ice extent for the study period 1978–2008 as derived from linear regression of the anomaly data points is close to zero at 0.8 ± 0.5%/decade. The trend in ice area is nearly double at 1.5 ± 0.5%/decade which is higher in part because the ice concentration has also been increasing at 0.6 ± 0.2%/decade. Since the trend for the combined sectors is small compared to the large positive trend of sea ice in the Ross Sea sector and the even larger negative trend in the Bellingshausen/Amundsen seas sector, the net trend is almost zero with the slight positive trend associated with the larger extent of the ice cover in the Ross Sea. In light of the large interannual variability, the processes in the two regions may be different and influenced by independent environmental forcing.

3.2. Sea Ice Drift, Interannual Variability, and Ice Export

[26] Sea ice drift data provide a powerful means to evaluate the ice dynamics as well as the sources and sinks of the sea ice cover. Ice motion from satellite passive microwave observations is derived using the procedure described in the work of *Kwok et al.* [1998]. The ice tracking makes use of the daily SSM/I 12.5 km resolution 85 GHz vertically polarized channels for the 17 year period 1992–2008, where only March–November data is used. The ice tracking results are less reliable during the austral summer and transitional months: this is due to variability in the brightness temperature fields associated with water vapor, cloud liquid water content and summer surface wetness. Even though 85 GHz data are available prior to 1992, they are not used because of the frequent coverage gaps. Monthly maps of sea level pressure (SLP) are computed from the NCEP/NCAR reanalysis [*Kalnay et al.*, 1996]. Figure 9, the mean monthly ice circulation for all months between April and November, shows that the domination of cyclonic drift pattern associated with a synoptic-scale low is centered over the Amundsen and northeast Ross seas. The drift pattern features a relatively weak inflow of sea ice into the Ross Sea from the east along the coast of the embayment, and a considerably stronger northwestward outflow.

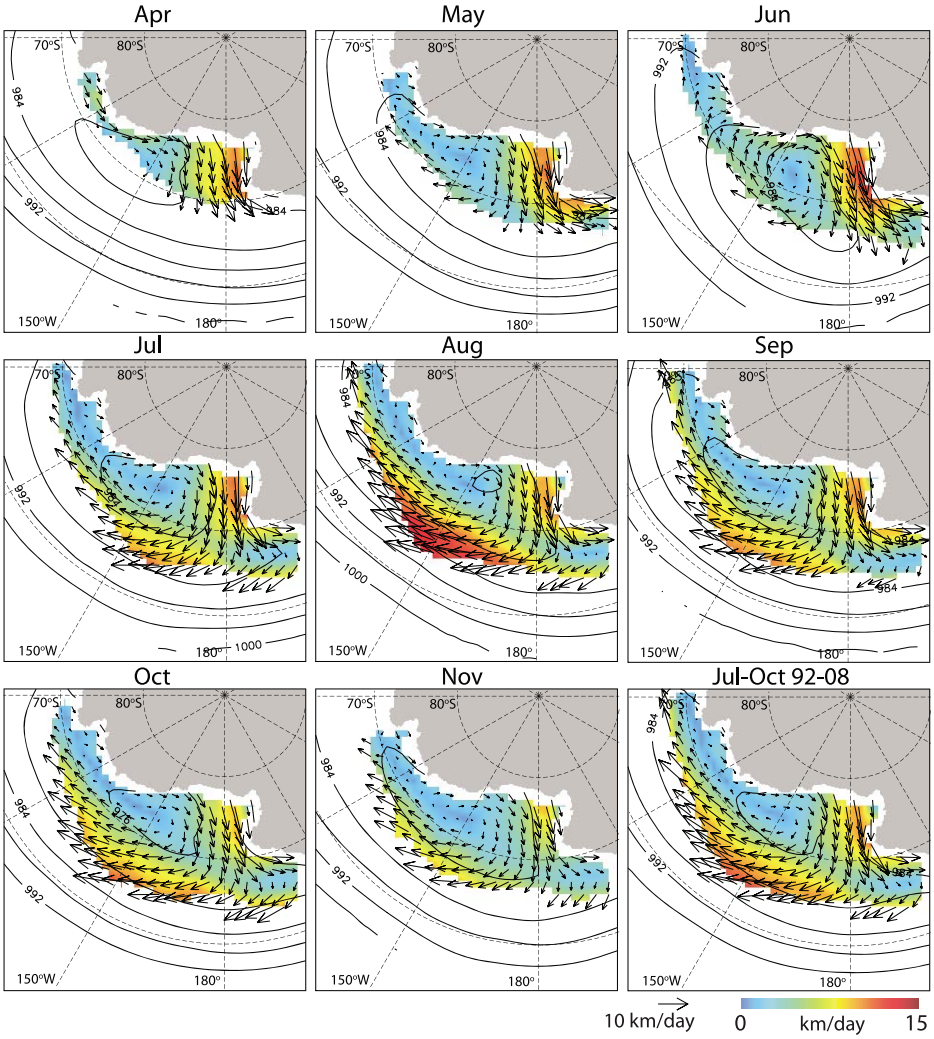

Figure 9. Ross Sea ice motion: 17 year mean ice motion (1992–2008) for the July–October period and mean monthly motion (1992–2006) for each month from April through November. Contour lines represent isobars of sea level pressure from NCEP-NCAR products (contour interval 4 hPa). March is not included in the mean fields because the ice coverage is small and vectors are sparse.

[27] In all the monthly fields shown in Figure 9, this larger northwest outflow of >10 km d^{-1} can be seen as a tongue (in red) that extends from the ice front of the Ross Ice Shelf to beyond Cape Adare. This imbalance between the inflow and outflow of ice occurs because of the significant production and export of sea ice associated with the Ross Sea polynyas. The katabatic flows and surges over the western Ross Ice Shelf are northward [*Savage and Stearns*, 1985], and appear to be the primary atmospheric forcing for development of these polynyas [*Bromwich et al.*, 1993] and the enhancement of the ice drift. About 60% of the polynya events are linked to katabatic surge events while the other 40% are linked to katabatic drainage winds from the Byrd, Skelton and Mulock glaciers and from barrier winds that flow northward along the Transantarctic Mountains and are deflected eastward by topographic barriers along the Scott Coast [*Bromwich et al.*, 1998].

[28] Depending on the location of the center of the low-pressure pattern, some recirculation of the outflow in the eastern Ross Sea is also evident. North of Cape Adare, the ice splits into two branches with one moving westward and the other northward. Farther north (<70°S), the prevailing motion is toward the east as the ice becomes entrained in the strong eastward flow of the Antarctic Circumpolar Current. At this latitude, the density of the sea level pressure isobars is much larger, with the average drift speed reaching >15 km d^{-1}.

[29] The interannual variability of the strength and pattern of the ice drift (1992–2008) can be seen in the mean July–October ice motion fields in Figure 10. The cyclonic pattern persists in all the winters. The features of the drift field, as described previously, are present in all the fields with their strength and spatial location dependent on the mean atmospheric low-pressure pattern. The tongue of northward drifting ice is wider when the center of the low is displaced eastward and the isobars are perpendicular to the ice front (e.g., 2000, 2001, and 2005). In contrast, the westward and northward displacements of this low (e.g., 1995, 2006)

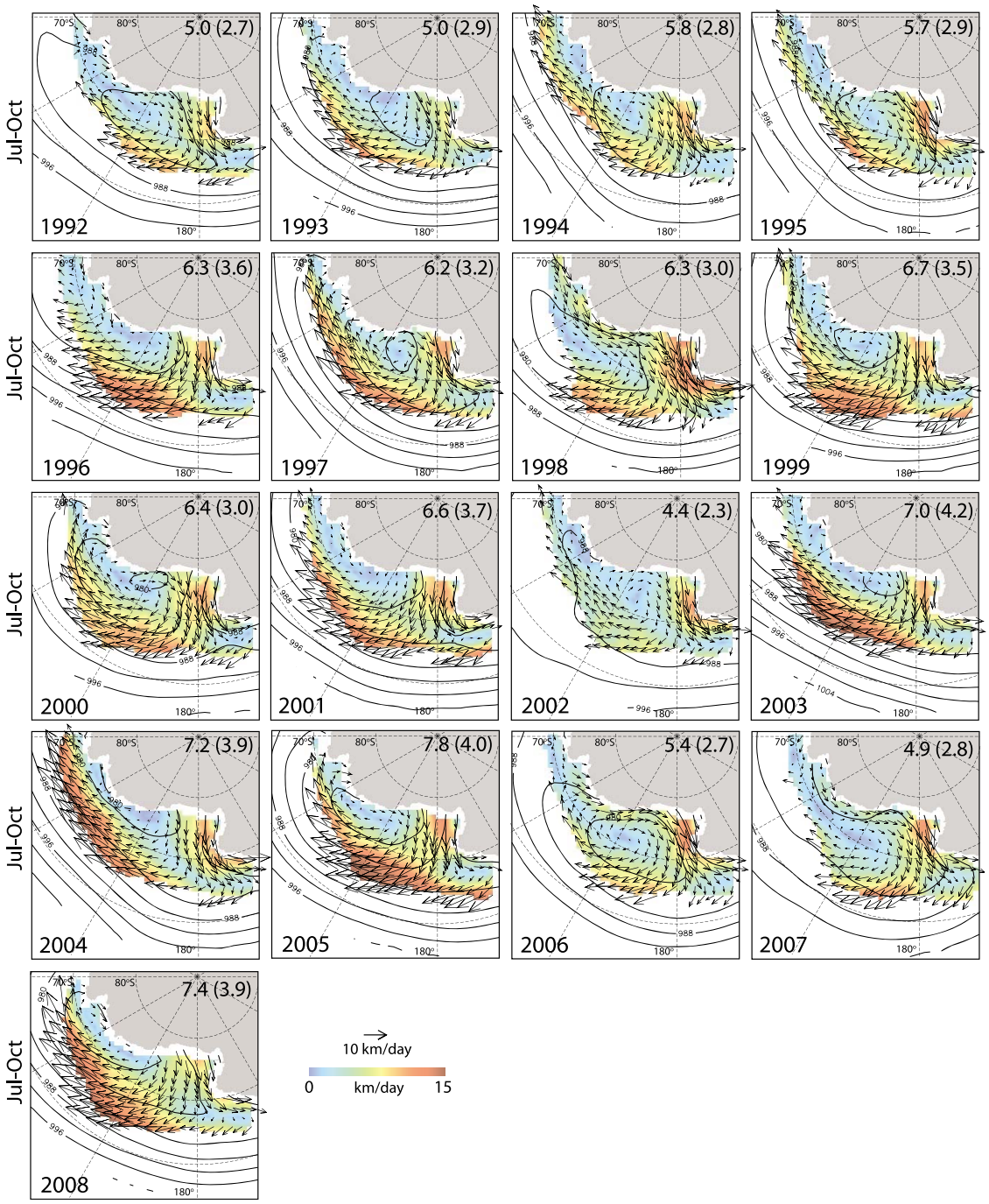

Figure 10. Interannual variability (1992–2008) of mean July–October ice motion in the Ross Sea. Isobars of sea level pressure from NCEP-NCAR products (contour interval 4 hPa). The quantities shown in the top right corners are the mean and standard deviation of the drift speed in km d^{-1} of the vectors within the domain.

increase the inflow into the Ross Sea and reduce the width of the outflow. The meridional displacement of the center of the low seems to control the width and speed of the inflow. In 2004, when the low-pressure center was displaced poleward, the typically offshore eastward ice drift is displaced southward and the westward inflow is not evident. This contributes to the high eastward drift speeds (7.2 km d^{-1}) seen that year. Together with the intensity of the low, the meridional and zonal displacements of its center seem to be the primary sources of interannual variability of the drift field.

[30] To examine sea ice outflow from the Ross Sea, we compute the ice flux across the fluxgate shown in Figure 11 as defined by *Kwok* [2005]. The eastern and western termini of the gate, with length of ~1400 km, are located at Land

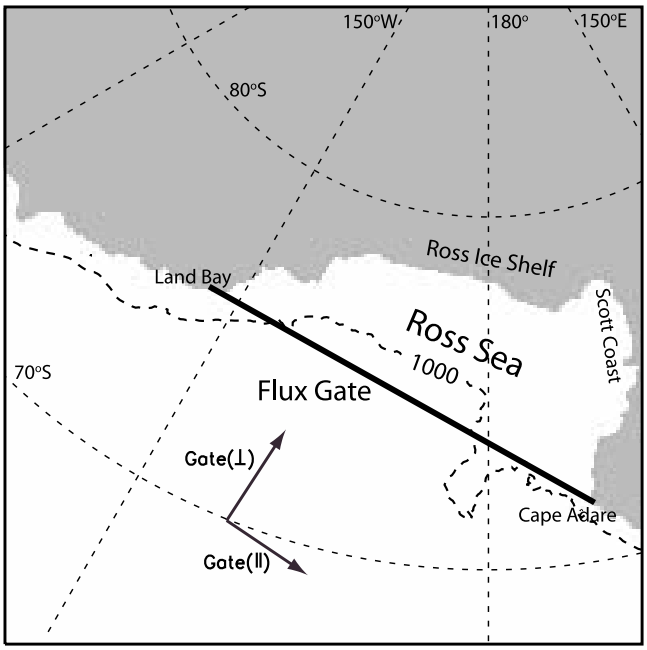

Figure 11. Ross Sea fluxgate, 1000 m isobath, and orientation of the gate coordinate system. The western endpoint of the gate is located at Cape Adare; the eastern at Land Bay. The length of the gate is 1400 km, and the enclosed area is ~490 × 10^3 km^2.

Bay and Cape Adare. We refer to the enclosed area (~490 × 10^3 km^2) as the Ross Sea. Following the procedure in the work of *Kwok and Rothrock* [1999], cross-gate motion profiles are created by first interpolating the gridded passive microwave ice motion to 50 uniformly spaced points (~28 km separation) along the ~1400 km gate. To avoid contamination by stationary land or ice pixels, ice motion vectors are not calculated within 50 km of the coast. Cubic splines, constrained to go to zero at the endpoints, are fitted to the two components of the motion vectors to fill gaps in the motion estimates along the gate. The vectors are then projected onto the unit normal of the fluxgate to obtain the magnitude of ice motion through the gate. The daily ice area outflow is then computed as the integral of the product of perpendicular ice motion and ice concentration along the gate.

[31] To examine the interannual variability of the inflow, outflow and net outflow at the area fluxgate over the 17 year record, we compute the winter area flux. We define this flux as the total of the daily 85 GHz area flux from the beginning of March until the end of November. For this period, Figure 12a presents the estimates for area inflow, outflow and net outflow, where the net area outflow is the difference between outflow and inflow. The average net area outflow over this period is 1.00 × 10^6 km^2 and ranges from a minimum of 0.50 × 10^6 km^2 in 1992 to a peak of 1.59 × 10^6 km^2 in 2001, a more than threefold variability. In 2001, the conditions that are favorable for large net outflow are the combination of the near perpendicular alignment of the isobars across the edge of the Ross Ice Shelf and the southeastward displacement of the center of the low. For this case, the net inflow of 0.35 × 10^6 km^2 is the smallest on record.

[32] Figure 12b shows the monthly inflow, outflow, and net outflow of ice area at the fluxgate. A positive net outflow would be a measure of the ice area produced in the Ross Sea if there were no melt or deformation of the sea ice advected into the area and the net production would be zero if export equals import. It is therefore of interest to examine the two contributions to the net outflow because it provides a rough estimate of the ice that is advected in from the east and the total exported in the west; that is, the ice area produced in the Ross Sea and the re-export of the eastern inflow. The mean monthly results show a definite seasonal cycle in outflow with a rapid increase in the early part of the winter followed by a slow decrease at the end of the ice growth season. It also shows that for the months shown here, the inflow seems to remain relatively constant compared to the outflow.

[33] In summary, the Ross Sea with an area of ~490 × 10^3 km^2 within the fluxgate, exports more than twice this area of sea ice every 9 months. The standard deviation of the winter flux, at 0.29 × 10^6 km^2, is large. A positive trend of ~30 × 10^3 km^2/winter can be seen in the 17 year record; however, the caveats in attributing significance to the trend of a relatively short data record apply. Using a mean Ross Sea spring ice thickness of 0.6 m [from *Jeffries and Adolphs*, 1997], we arrive at a positive trend in the volume ice export of ~20 km^3/winter. The net positive trend during the 17 years appears to be the result of a positive trend in the total outflow and a smaller negative trend in the inflow. In general, the interannual variability of net area outflow is similar to that of the sea ice extent (Figures 7e and 8d). For example, low values in 1992, 1995 and 1997 and a high value in 1999 occur in both data sets. During the 1992–2008 period, the trends in both data sets are positive. Significant discrepancies are apparent primarily because the area outflow depends on the gradient in the SLP near the fluxgate (i.e., the density of isobars perpendicular to the gate) while the ice extent depends primarily on the meridional ice velocity further out toward the ice edge. Thus the entire system is dependent on the location, shape and depth of the low-pressure trough centered over the eastern Ross Sea.

[34] In 2001, there is no match in the regional ice extent in the anomaly map in Figure 5 to the large value in the area outflow. This was because the gradient along the fluxgate in 2001 was large (large ice flux), while the zonal component of the ice velocity near the ice edge is much greater than the meridional component because the center of that trough in the velocity field is displaced east and landward. Also, in 2007, the ice extent was relatively large and the ice anomaly in winter was very positive while the plot of the net outflow shows a relatively low value. During this year, the meridional ice velocity was large near the ice edge while the gradient in SLP was low near the fluxgate (i.e., low ice velocities). This means that the variability of the sea ice cover in the Ross Sea cannot be explained solely by the advection of ice through the fluxgate. One difficulty with the areal ice export estimate is that by necessity, it ignores the interannual changes in thickness of the exported ice. Variations in mean thickness

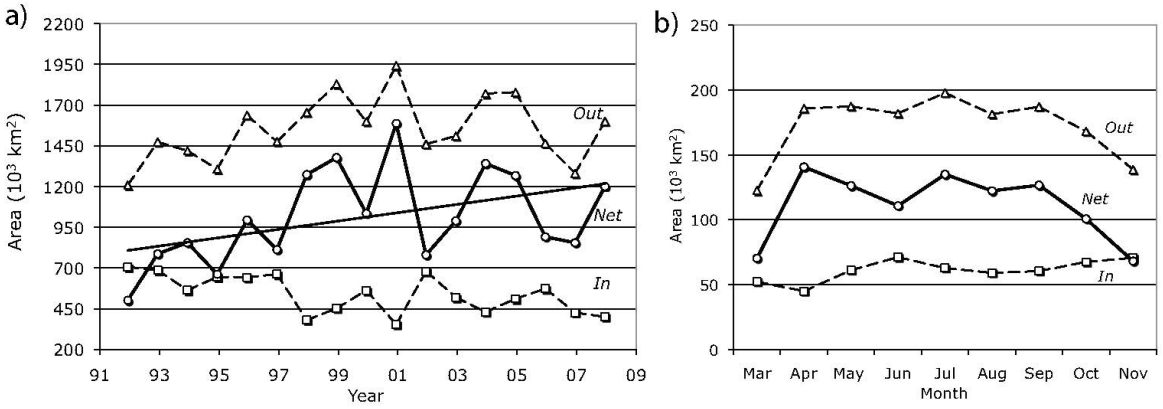

Figure 12. Ice area inflow, total outflow, and net outflow through the fluxgate, as illustrated in Figure 11, for (a) each winter (March to November average from 1992 to 2008) and (b) the multiyear monthly mean between March and November.

from year-to-year would change the total volume exported, independent of the net areal export.

4. Polynya Formation, Salinization, and Ice Production

[35] The Ross Sea is uniquely suited for the production of high-density bottom water because of its wide continental shelf, and the enormous recurring RSP and the smaller Terra Nova Bay polynya. Coastal polynyas in the Ross Sea have been studied previously using passive microwave data [*Zwally et al.*, 1985; *Cavalieri and Martin*, 1985; *Jacobs and Comiso*, 1989] and more recently using SAR, passive microwave and other data sets [*Martin et al.*, 2007; *Kwok et al.*, 2007; *Tamura et al.*, 2008; *Kern*, 2009]. The coastal polynyas form primarily as a result of strong southerly winds that cause the advection of ice to the north as described in section 3.2. The size of the polynyas depends on the persistence and strength of the winds that vary on a daily and seasonal basis. Their largest ice productivity occurs in the austral autumn and winter. The polynyas occur anytime, but toward the end of the spring, they start to grow larger concurrently with the ice breakup. As discussed by *Smith and Comiso* [2008], because of the regional melt of sea ice, the spring polynyas have been identified as regions of high biological primary productivity. They also provide indirect information about the conditioning of the region that may be associated with the occurrence of polynyas during the previous winter.

[36] Following *Martin et al.* [2007], we calculate the ice production in the coastal polynyas using the 37 GHz thin ice algorithm that *Martin et al.* [2004] describe and validate against AVHRR data for both area and heat flux, and *Martin et al.* [2005] validate against SAR data for area only. Our current study period is 1992–2008, where our analysis uses the daily SSM/I and ECMWF data sets. For 2003–2008, we use the same thin ice algorithm to additionally calculate the ice production from the AMSR-E 36 GHz 12.5 km resolution data. Because of problems with missing data and sidelobe contamination [*Martin*, 2004, chapter 8], we do not extend this series back into the 1978 to 1987 SMMR period.

[37] Figure 13 shows on the left-hand scale, the annual polynya ice productivity in km^3 for the RSP, which is by far the dominant Ross Sea polynya. As described in the work of *Martin et al.* [2007], Figure 13 also takes into account the effect of icebergs B15 (which broke into B15A, B15B) and C19 in the altering and enhancing the ice production in 2000 and 2002. In the analysis, icebergs must be masked because they have a microwave signature similar to thin ice. In their derivation of this mask, *Martin et al.* [2007] use near daily MODIS (moderate imaging spectrophotometer) imagery to derive a time series of the iceberg positions, sizes and orientations that are used to mask the passive microwave data. Also, *Martin et al.* [2007] and the present paper take into account not only the polynya that occurred downwind of the ice shelf, but also the polynyas that occurred downwind of the iceberg fragments. In 2000, this inclusion of the iceberg polynyas enhances the total ice production.

[38] The error bars on the ice production are derived as follows: In their validation of the SSM/I algorithm, *Martin et al.* [2004] compare the heat fluxes calculated from the SSM/I and from the 1 km resolution AVHRR set of pixels that fill the SSM/I pixels, then treating the AVHRR as the correct result, find that the root mean square accuracy of SSM/I heat fluxes relative to the AVHRR heat fluxes is about 20%. The vertical lines show these error bars on the SSM/I time series, the error bars neglect the fact that the large passive microwave pixels tend to underestimate the polynya area. For 2003–2008, the six points connected by the dashed lines show the AMSR-E results; because of their better resolution, these lie above the SSM/I points. The linear least squares fit to the SSM/I points shows that over the 17 year period, the ice production doubles from 300 to 600 km^3 yr^{-1}, or increases at a rate of about 20 km^3 yr^{-1}. Within error bars, this increase agrees with that estimated from the areal ice export in section 3.2.

[39] Figure 13 shows that the ice production exhibits interannual fluctuations with peaks in 2000, 2005, and 2007, and minima in 1993, 1997, 2002, and 2006. For the net ice outflow shown in Figure 12, the strongest maxima or near maxima occur in 1999, 2001, 2004, and 2005, so that although both time series show an upward trend, the respective peaks

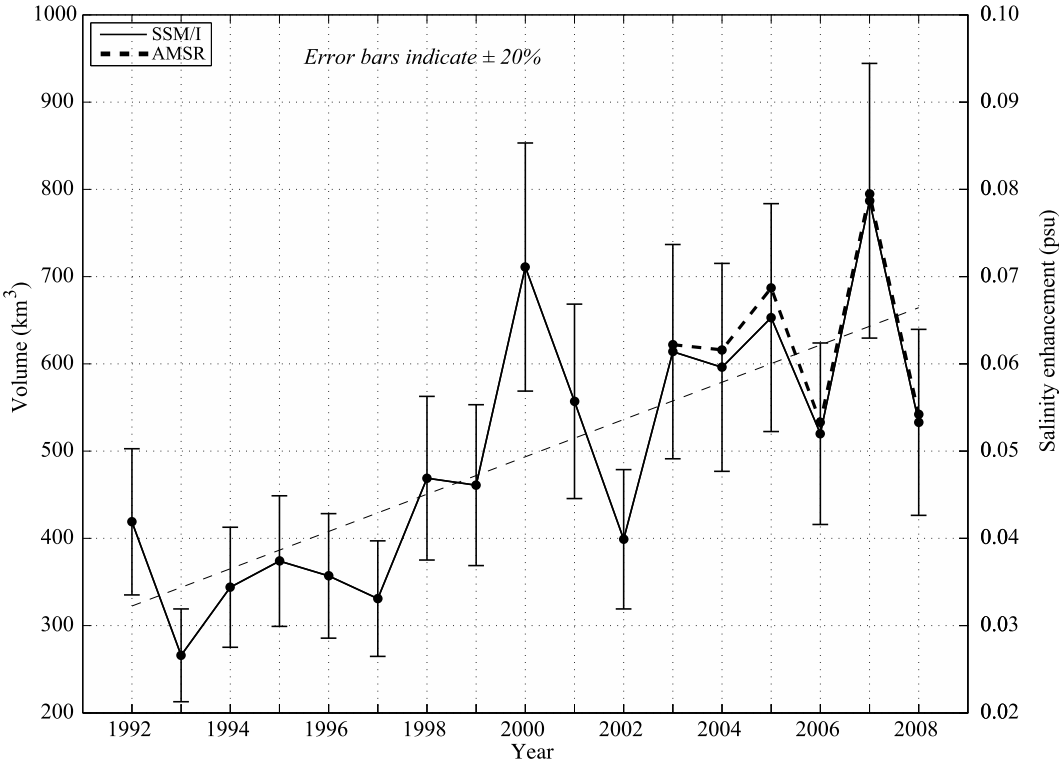

Figure 13. Annual values of ice production and salinity enhancement from the Ross Sea polynya from 1992 to 2008. The curves are identical for both parameters with the ice production axis on the left and the salinity axis on the right. See text for further description.

and valleys do not match. This lack of agreement may be caused by our attempt to equate ice volume with ice area without knowledge of the interannual variability of the ice thickness, so that the net ice export is not necessarily a linear function of the polynya ice production.

[40] From this ice production time series, we estimate the salinity enhancement as follows. First, we assume that the salt rejected from the polynya ice growth is mixed uniformly to a depth of 500 m within the area of the Ross Sea defined by the fluxgate (490×10^3 km^2). For a surface salinity of 34 psu, we convert the volume of ice growth to its equivalent volume of seawater. Following *Skogseth et al.* [2004], we then assume that 79% of the salt is rejected, and that the rejected amount is spread out uniformly over the 500 m water depth. From the SSM/I and AMSR-E ice production values, we then obtain the annual salinity enhancements shown by the right-hand scale of Figure 13, where from the above assumptions, the ice production and salinity enhancement follow identical curves. The salinity enhancement has a minimum of 0.034 psu, a maximum of 0.093 psu and a linear trend of +0.023 psu/decade. In contrast, *Jacobs and Giulivi* [2010] report that from 1958 to 2008, the shelf salinity in the southwest Ross Sea declined at a rate of −0.03/decade, so that the observed trend is similar in magnitude but opposite in sign to the calculated.

[41] *Kern* [2009] and *Tamura et al.* [2008] also study the RSP, but obtain different results. For 1992–2008, *Kern* [2009] who considers only polynya areas, finds that the area of the RSP is nearly constant. However, he calculates his areas only for the 4 month period of June–September, even though he acknowledges that this time restriction "misses the commonly larger polynya areas during the beginning of winter." In contrast, we begin our area and ice production calculations at that time when the ice cover fills our region of interest, and end it when the ice production approaches zero. In our case, both the start and end dates vary; over the 17 year period, the start date occurs at various times in March, and the end dates occur in early November, yielding an ~8 month period, or twice that of Kern. Since we use an 8 month analysis period and variable start and stop dates while Kern uses a 4 month period, we feel that his results are not comparable with ours.

[42] A major difference between the results presented in this paper and those in the work of *Tamura et al.* [2008] is apparent. In particular, *Tamura et al.* [2008] showed a 35% step decrease in ice production between 1999 and 2000, while for the same 2 years, our Figure 13 shows a 38% increase, and *Martin et al.* [2007, Figure 11] find a 30% increase. *Tamura et al.* [2008] derive their annual ice production between March and October, independent of the ice conditions at the beginning of the time series, which would generate only a slightly different result from ours. Their iceberg masks are derived differently from ours; they determine whether a point should be masked as an iceberg from values determined from a scatterplot analysis of their passive microwave data. Because they do not give information about how they validated this technique, especially for moving icebergs, we assume that their determination of the iceberg masks is less accurate than our independent derivation from MODIS data. It is also not clear from their

paper if they include the polynyas that form downwind of the icebergs, or instead include only that part of the polynya that occurs adjacent to the ice shelf. In summary, we feel that the cause of our production increase between 1999 and 2000 and the decrease reported by *Tamura et al.* [2008] is a function of the different methods used to derive the iceberg masks, and of our taking into consideration the secondary polynyas that form downwind of the icebergs.

[43] The use of the ERA-40 data set in the work of *Martin et al.* [2007] and the ECMWF operational data set in the current paper creates some differences in the ice production between the two papers, most notably in the year 2000, where the ice production in the current paper is 180 km^3 greater. This difference is not unusual, when *Tamura et al.* [2008, Figure 2a] compare their ice production as derived from ERA-40 and from NCEP2 (National Center for Environmental Prediction2), they find differences of about 100 km^3, with the ERA-40 producing the smaller estimates.

[44] The question remains, why do we predict an increase in ice production that is consistent with the net ice export described in section 3.2, while the salinity increase is inconsistent with the observed HSSW salinity decrease? We suggest the following answer. The HSSW salinity responds to both the local salt rejection and to the salinity of the water advected into the region from the Amundsen Sea as well as to the regional glacial ice meltwater. *Jacobs and Giulivi* [2010] discuss this dependence and show a positive trend in freshening of the Amundsen Seawaters since the 1990s, a consequence of increased precipitation and decreased sea ice export, as well as regional dilution by glacial meltwater. The freshening of the inflow into the Ross Sea from the Amundsen Sea as well as Ross Ice Shelf melting act to compensate the salt input by the sea ice export from the Ross Sea. Of course, the interpretation of trends, especially when the yearly variations are large and the record length is relatively short, need to be considered with caution.

5. Discussion and Conclusions

[45] The sea ice cover in the Antarctic is studied using 30 years of satellite data with a view of gaining insights into the unexpected positive trend in the sea ice extent in the Southern Ocean and the overall cooling. The focus of the study is the Ross Sea sector that is primarily responsible for the positive trend. While the trend in the ice cover in the Bellingshausen/Amundsen seas sector is about −7% per decade, the trend in the Ross Sea ice sector, which has a greater ice extent than the former, is 5% per decade. For the combined sectors, the trend in extent is small at about 0.8% per decade. It is thus possible that with the absence of a natural boundary, the different trends observed from the two sectors are in part caused by the advection of sea ice from one sector to another. The Ross Sea also has an ice factory in its polynyas where changes in wind circulation alter ice production.

[46] The climate of the two regions however, is very different in that the Bellingshausen region is warming while the Ross is experiencing significant cooling. The circumpolar ice cover has also been analyzed to evaluate the possible contribution of the Antarctic Circumpolar Wave (ACW) to the observed interannual variability in the region. For 1981 to 1989, the ACW shows some characteristics that are consistent with a mode 2 propagating wave. Four years later when the pattern is expected to repeat, the pattern is not as consistent and the inconsistencies continue for subsequent years. The inconsistencies may be due in part to frequent occurrences of a mode 3 wave compared to the expected mode 2. It is also obvious that since 1998, and except in 2003 and in a minor way in 2001 and 2004, the Ross Sea ice edge was further to the north than average.

[47] Satellite ice drift data in the region has been analyzed and for the period 1992 to 2008, an area in the inner Ross Sea of ~490 × 10^3 km^2 within the fluxgate exports more than twice its own area of sea ice during the 9 months of ice growth each year. Although the standard deviation of the flux, at 0.29 × 10^6 km^2, is large, a positive trend of ~30 × 10^3 km^2/winter is inferred. During the 17 year observational period, the net positive trend appears to be the result of a positive trend in the total outflow and a smaller negative trend in the area inflow. For a documented average ice thickness in the Ross Sea of 0.6 m, this trend becomes ~20 km^3 yr^{-1}.

[48] For the Ross Shelf Polynya, the total ice production and salinization has been estimated for each year from 1992 to 2008 from daily brightness temperature data. The estimates were made using an ice production algorithm based on the daily ECMWF weather and SSM/I data. The results show that the ice production and salinization, with considerable variability, increase with time, where a linear trend fit to the ice production also yields ~20 km^3 yr^{-1}. For the 17 year period, this increase in ice production matches within error bars, the yearly trend in ice transport from the region as inferred from the ice drift data and is consistent with the general increase in the Ross sea ice area. The relatively short data record requires some caution in interpreting the results.

[49] The question arises as to why the enhanced salt production associated the increase in ice production does not lead to an observed increase in the salinity of the Ross seawater column. Here we point out that the Ross Sea salinity is not simply determined by the local sea ice budget, but rather by a combination of sea ice factors and the advection of lower-salinity water, owing to excess of precipitation over evaporation and regional glacial ice melt from neighboring seas, notably from the Amundsen Sea, as well as within the Ross Sea. Thus while the increase in sea ice production would cause an increase in the production of HSSW (or make it more saline) it is insufficient to offset the import of low-salinity shelf water from the Bellingshausen/Amundsen seas, and therefore does not result in greater bottom water production in the Ross Sea. These results are intriguing but should be treated with caution because of the large interannual variability of environmental conditions and the relatively short record length.

[50] **Acknowledgments.** J.C.C. would like to thank Robert Gerstein for programming support in the analysis of SSM/I and AMSR-E data and is grateful to the NASA Cryospheric Sciences Program for funding support. S.M. thanks Robert Drucker for his help with Figure 13 and gratefully acknowledges the support of NASA under contract NNG04GM69G. R.K. performed this work at the Jet Propulsion Laboratory, California Institute of Technology, under contract with NASA. A.L.G.'s support is from the National Science Foundation Office of the Polar Programs grant ANT-0538148, Lamont-Doherty contribution number 7397. We all thank the National Snow and Ice Data Center for provision of the SMMR, SSM/I

and AMSR-E data. The ECMWF meteorological products are provided by the Data Support Section of the Scientific Computing Division of the National Center for Atmospheric Research (NCAR). NCAR is supported by grants from the National Science Foundation.

References

Bromwich, D. H., and D. D. Kurtz (1982), Experiences of Scott's Northern Party: Evidence for a relationship between winter katabatic winds and the Terra Nova Bay Polynya, *Polar Rec.*, *21*, 137–146, doi:10.1017/S0032247400004514.

Bromwich, D. H., and D. D. Kurtz (1984), Katabatic wind forcing of the Terra Nova Bay polynya, *J. Geophys. Res.*, *89*, 3561–3572, doi:10.1029/JC089iC03p03561.

Bromwich, D. H., J. F. Carrasco, Z. Liu, and R. Y. Tzeng (1993), Hemispheric atmospheric variations and oceanographic impacts associated with katabatic surges across the Ross Ice Shelf, Antarctica, *J. Geophys. Res.*, *98*, 13,045–13,062, doi:10.1029/93JD00562.

Bromwich, D. H., Z. Liu, A. N. Rogers, and M. L. Van Woert (1998), Winter atmospheric forcing of the Ross Sea polynya, in *Oceans, Ice and Atmosphere: Interactions at the Antarctic Continental Margin*, *Antarct. Res. Ser.*, vol. 75, edited by S. Jacobs and R. Weiss, pp. 101–133, AGU, Washington, D. C.

Budillon, G., M. Pacciaroni, S. Cozzi, P. Rivaro, G. Catalano, C. Ianni, and C. Cantoni (2003), An optimum multiparameter mixing analysis of the shelf waters in the Ross Sea, *Antarct. Sci.*, *15*, 105–118, doi:10.1017/S095410200300110X.

Cavalieri, D. J., and S. Martin (1985), A passive microwave study of polynyas along the Antarctic Wilkes Land Coast, in *Oceanology of the Antarctic Continental Shelf*, *Antarct. Res. Ser.*, vol. 43, edited by S. Jacobs, pp. 203–226, AGU, Washington, D. C.

Comiso, J. C. (2009), Enhanced sea ice concentration and ice extent from AMSR-E, *J, Remote Sens. Soc. Jpn.*, *29*, 199–215.

Comiso, J. C. (2010), *Polar Oceans From Space*, 507 pp., Springer, New York.

Comiso, J. C., and F. Nishio (2008), Trends in the sea ice cover using enhanced and compatible AMSR-E, SSM/I, and SMMR data, *J. Geophys. Res.*, *113*, C02S07, doi:10.1029/2007JC004257.

Defense Mapping Agency (1992), Military specification—Digital chart of the world, *Rep. MIL-D 89009*, 204 pp., Def. Print. Serv., Philadelphia, Pa.

Fusco, G., G. Budillon, and G. Spezie (2009), Surface heat fluxes and thermohaline variability in the Ross Sea and in Terra Nova Bay polynyas, *Cont. Shelf Res.*, *29*, 1887–1895, doi:10.1016/j.csr.2009.07.006.

Gille, S. T. (2002), Warming of the Southern Ocean since the 1950s, *Science*, *295*, 1275–1277.

Gordon, A. L., E. Molinelli, and T. Baker (1978), Large-scale relative dynamic topography of the Southern Ocean, *J. Geophys. Res.*, *83*, 3023–3032.

Gordon, A. L., A. H. Orsi, R. Muench, B. A. Huber, E. Zambianchi, and M. Visbeck (2009), Western Ross Sea continental slope gravity currents, *Deep Sea Res. Part II*, *56*, 796–817, doi:10.1016/j.dsr2.2008.10.037.

Hall, A., and M. Visbeck (2002), Synchronous variability in the Southern Hemisphere atmosphere, sea ice, and ocean resulting from the Annular Mode, *J. Clim.*, *15*, 3043–3057.

Jacobs, S. S., and J. C. Comiso (1989), Satellite passive microwave sea ice observations and oceanic processes in the Ross Sea, Antarctica, *J. Geophys. Res.*, *94*, 18,195–18,211, doi:10.1029/JC094iC12p18195.

Jacobs, S. S., and J. C. Comiso (1997), Climate variability in the Amundsen and Bellingshausen seas, *J. Clim.*, *10*, 697–709, doi:10.1175/1520-0442(1997)010<0697:CVITAA>2.0.CO;2.

Jacobs, S. S., and C. F. Giulivi (2010), Large multi-decadal salinity trends near the Pacific-Antarctic Continental Margin, *J. Clim.*, *23*, 4508–4524, doi:10.1175/2010JCLI3284.1.

Jeffries, M. O., and U. Adolphs (1997), Early winter ice and snow thickness distribution, ice structure and development of the western Ross Sea pack ice between the ice edge and the Ross Ice Shelf, *Antarct. Sci.*, *9*, 188–200.

Kalnay, E., et al. (1996), The NCEP/NCAR 40-year reanalysis project, *Bull. Am. Meteorol. Soc.*, *77*, 437–471.

Kern, S. (2009), Wintertime Antarctic coastal polynya area: 1992–2008, *Geophys. Res. Lett.*, *36*, L14501, doi:10.1029/2009GL038062.

King, J. C., and S. A. Harangozo (1998), Climate change in the western Antarctic Peninsula since 1945: Observations and possible causes, *Ann. Glaciol.*, *27*, 571–575.

Kwok, R. (2005), Ross sea ice motion, area flux and deformation, *J. Clim.*, *18*, 3759–3776.

Kwok, R., and J. C. Comiso (2002), Spatial patterns of variability in Antarctic surface temperature: Connections to the Southern Hemisphere Annular Mode and the Southern Oscillation, *Geophys. Res. Lett.*, *29*(14), 1705, doi:10.1029/2002GL015415.

Kwok, R., and D. A. Rothrock (1999), Variability of Fram Strait ice flux and North Atlantic Oscillation, *J. Geophy. Res.*, *104*, 5177–5189.

Kwok, R., A. Schweiger, D. A. Rothrock, S. Pang, and C. Kottmeier (1998), Sea ice motion from satellite passive microwave data assessed with ERS SAR and buoy data, *J. Geophys. Res.*, *103*, 8191–8214, doi:10.1029/97JC03334.

Kwok, R., J. C. Comiso, S. Martin, and R. Drucker (2007), Ross Sea polynyas: Response of ice concentration retrievals to large areas of thin ice, *J. Geophys. Res.*, *112*, C12012, doi:10.1029/2006JC003967.

Ledley, T. S., and Z. Huang (1997), A possible ENSO signal in the Ross Sea, *Geophys. Res. Lett.*, *24*, 3253–3256, doi:10.1029/97GL03315.

Markus, T., and D. J. Cavalieri (2009), The AMSR-E NT2 Sea ice concentration algorithm: Its basis and implementation, *Remote Sens. Soc. Jpn.*, *29*, 216–223.

Martin, S. (2004), *An Introduction to Ocean Remote Sensing*, 426 pp., Cambridge Univ. Press, New York.

Martin, S., R. Drucker, R. Kwok, and B. Holt (2004), Estimation of the thin ice thickness and heat flux for the Chukchi Sea Alaskan coast polynya from SSM/I data, 1990–2001, *J. Geophys. Res.*, *109*, C10012, doi:10.1029/2004JC002428.

Martin, S., R. Drucker, R. Kwok, and B. Holt (2005), Improvements in the estimates of ice thickness and production in the Chukchi Sea polynyas derived from AMSR-E, *Geophys. Res. Lett.*, *32*, L05505, doi:10.1029/2004GL022013.

Martin, S., R. S. Drucker, and R. Kwok (2007), The areas and ice production of the western and central Ross Sea polynyas, 1992–2002, and their relation to the B-15 and C-19 iceberg events of 2000 and 2002, *J. Mar. Syst.*, *68*, 201–214, doi:10.1016/j.jmarsys.2006.11.008.

Massom, R. A., S. E. Stammerjohn, W. Lefebvre, S. A. Harangozo, N. Adams, T. A. Scambos, M. J. Pook, and C. Fowler (2008), West Antarctic Peninsula sea ice in 2005: Extreme ice compaction and ice edge retreat due to strong anomaly with respect to climate, *J. Geophys. Res.*, *113*, C02S20, doi:10.1029/2007JC004239.

Orsi, A. H., and C. L. Wiederwohl (2009), A recount of Ross Sea waters, *Deep Sea Res. Part II*, *56*, 778–795, doi:10.1016/j.dsr2.2008.10.033.

Parkinson, C. L., and J. C. Comiso (2008), Antarctic sea ice from AMSR-E from two algorithms and comparisons with sea ice from SSM/I, *J. Geophys. Res.*, *113*, C02S06, doi:10.1029/2007JC004253.

Savage, M. L., and C. R. Stearns (1985), Climate in the vicinity of Ross Island, Antarctica, *Antarct. J.*, *20*, 1–9.

Skogseth, R., P. M. Haugan, and J. Haarpaintner (2004), Ice and brine production in Storfjorden from four winters of satellite and in situ observations and modeling, *J. Geophys. Res.*, *109*, C10008, doi:10.1029/2004JC002384.

Smith, W. O., Jr., and J. C. Comiso (2008), The influence of sea ice primary production in the Southern Ocean: A satellite perspective, *J. Geophys. Res.*, *113*, C05S93, doi:10.1029/2007JC004251.

Stammerjohn, S. E., D. G. Martinson, R. C. Smith, X. Yuan, and D. Rind (2008), Trends in Antarctic annual sea ice retreat and advance and their relation to El Niño–Southern Oscillation and Southern Annular Mode variability, *J. Geophys. Res.*, *113*, C03S90, doi:10.1029/2007JC004269.

Steig, E. J., D. P. Schneider, S. D. Rutherford, M. E. Mann, and J. C. Comiso (2009), Warming of the Antarctic ice sheet surface since the 1957 International Geophysical Year, *Nature*, *457*, 459–462, doi:10.1038/nature07669.

Tamura, T., K. I. Ohshima, and S. Nihashi (2008), Mapping of sea ice production for Antarctic coastal polynyas, *Geophys. Res. Lett.*, *35*, L07606, doi:10.1029/2007GL032903.

Thompson, D. W., and J. S. Solomon (2002), Interpretation of recent Southern Hemisphere climate change, *Science*, *296*, 895–899, doi:10.1126/science.1069270.

Turner, J., J. C. Comiso, G. J. Marshall, W. M. Connolley, T. A. Lachlan-Cope, T. Bracegirdle, Z. Wang, M. Meredith, and T. Maksym (2009), Antarctic sea ice extent increases as a result of anthropogenic activity, *Geophys. Res. Lett.*, *36*, L08502, doi:10.1029/2009GL037524.

White, W. B., and R. G. Peterson (1996), An Antarctic circumpolar wave in surface pressure, wind, temperature and sea-ice extent, *Nature*, *380*, 699–702, doi:10.1038/380699a0.

Yuan, X., and C. Li (2008), Climate modes in southern high latitudes and their impacts on Antarctic sea ice, *J. Geophys. Res.*, *113*, C06S91, doi:10.1029/2006JC004067.

Zwally, H. J., J. C. Comiso, C. L. Parkinson, W. J. Campbell, F. D. Carsey, and P. Gloersen (1983), Antarctic sea ice, 1973–1976: Satellite passive-microwave observations, report, 213 pp., Sci. and Tech. Inf. Branch, NASA, Washington, D. C.

Zwally, H. J., J. C. Comiso, and A. L. Gordon (1985), Antarctic offshore leads and polynyas and oceanographic effects, in *Oceanology of the Antarctic Continental Shelf*, *Antarct. Res. Ser.*, vol. 43, edited by S. Jacobs, pp. 203–226, AGU, Washington, D. C.

Zwally, H. J., J. C. Comiso, C. L. Parkinson, D. J. Cavalieri, and P. Gloersen (2002), Variability of Antarctic sea ice 1979–1998, *J. Geophys. Res.*, *107*(C5), 3041, doi:10.1029/2000JC000733.

J. C. Comiso, Cryospheric Sciences Branch, NASA Goddard Space Flight Center, 8800 Greenbelt Rd., Code 614.1, Greenbelt, MD 20771, USA. (josefino.c.comiso@nasa.gov)

R. Kwok, Jet Propulsion Laboratory, California Institute of Technology, 4800 Oak Grove Dr., Pasadena, CA 91109, USA.

A. L. Gordon, Lamont-Doherty Earth Observatory, Columbia University, PO Box 1000, 61 Route 9W, Palisades, NY 10964, USA.

S. Martin, School of Oceanography, University of Washington, Box 357940, Seattle, WA 98195-7940, USA.